This is a draft of the following article, which is available from http://octadlab.ust.hk

J. M. Shihua, R. P. Liem and Y. Li. An Improved Experimental Framework of Amphibious Marine Vehicle Hull Hydrodynamics. IEEE Journal of Oceanic Engineering, doi: 10.1109/JOE.2023.3303956.

The published article may differ from this draft.

An Improved Experimental Framework of Amphibious Marine Vehicle Hull Hydrodynamics

James M. Shihua* Rhea P. Liem† Ye Li‡

Abstract With the increase of anthropogenic oceanic activities, a great number of innovative marine vehicles have been proposed and developed in the past few decades. Among these new vehicles, amphibious marine vehicle is considered as one of the most unique as it operates in air and water. This unique mode of operation necessitates simultaneous and coupled analyses of the aerodynamic and hydrodynamic performances. However, most of existing methods are still not able to separate and resolve the hydrodynamic behaviour of the hull from the coupled system, which hinders in-depth research and development of such vehicles. To advance the understanding of the amphibious vehicle and support a more comprehensive design process, in this paper, we propose an improved experimental framework that can decouple the hydrodynamics and aerodynamics effects. As a result, the hydrodynamic performance data retrieved under this framework can be scaled to a prototype by Froude's similarity law. Using a scaled model, a comparative analysis is performed to demonstrate the advantages of the new framework. Results show that the new framework not only can isolate aerodynamics and hydrodynamics loads from each other, but also provides a more scalable and reliable resistance coefficient compared with those obtained from existing frameworks. Furthermore, this framework can also reveal more detailed hydroplaning lift characteristics, which constitute a crucial feature in amphibious vehicle analysis. Moving forward, this new framework is expected to serve as a more accurate platform to derive a data-enhanced explanatory model which will facilitate multidisciplinary design and optimization on an amphibious marine vehicle.

*PhD Candidate, Department of Mechanical and Aerospace Engineering, Hong Kong University of Science and Technology.

†Associate Professor, Department of Mechanical and Aerospace Engineering, Hong Kong University of Science and Technology.

‡Professor, School of Naval Architecture, Ocean & Civil Engineering, Shanghai Jiao Tong University, Shanghai.

Nomenclature

C_L	=	Hydroplaning force coefficient $\frac{L}{\rho g b^3}$
C_V	=	Speed coefficient $\frac{V}{\sqrt{gb}}$
C_R	=	Resistance coefficient $\frac{R}{\rho g b^3}$
C_Δ	=	Load coefficient $\frac{\Delta}{\rho g b^3}$
Fr	=	Froude number $\frac{V}{\sqrt{gL}}$
Re	=	Reynolds number $\frac{\rho V L}{\mu}$
H	=	Hydroplaning lift (N)
L	=	Aerodynamic lift (N)
R	=	(Total) hydrodynamic resistance (N)
S_{wet}	=	Wetted surface area (m^2)
V	=	Speed (m/s)
Δ	=	Buoyancy load (N)
b	=	Maximum beam (width) of hull (m)
ρ	=	Density of water (kg/m^3)
τ	=	Trim angle, angle between keel and waterline (°)

Subscripts

f	=	Skin friction
m	=	Scaled model
w	=	Wave-making
s	=	Full-scale prototype

Abbreviation

NACA	=	National Advisory Committee for Aeronautics
ITTC	=	International Towing Tank Conference
WIG	=	Wing-in-ground
STOL	=	Short takeoff and landing

1 Introduction

With the ever-increasing human activities and utilization involving the ocean, the development of marine technology and engineering receives great attention, in which, marine vehicles play an important role [1]. In particular, an increasing number of unconventional marine vehicles have been gradually introduced, including amphibious aircraft [2], wing-in-ground (WIG) craft [3], unmanned surface vehicles [4], and autonomous underwater vehicle [5], to name a few. Most of them are operated in a single medium, such as underwater or on water surface, and usually at moderate

speed. However, some more challenging contemporary maritime applications (such as coastal petrol and surveillance, monitoring of offshore engineering facilities [6, 7]) demand a vehicle that possesses more agility, adaptability, and versatility. Addressing these needs requires assistance from auxiliary facilities such as tugs or cranes [8], or the development of a marine vehicle with a high operating speed that is comparable to a general aviation aircraft of similar size and, at the same time, the ability to perform tasks on water surface [9]. It is believed that the latter solution is more cost-effective for the future [10].

An amphibious marine vehicle refers to a vehicle that can operate both on water surface and in the air. As such, it requires components of a ship in addition to those typical of an aircraft (see a simple schematic illustrated in Fig. 1). It was first introduced in the 1910s [11] and became popular until the World War II [12] (see Table 1 for major development prototypes). Most development programs, however, were terminated with the advent of jet era, due to an overwhelming need in the commercial aviation market. In recent years, amphibious marine vehicles start gaining interests in countries with extensive coastal lines, such as Japan, China, Russia, etc. [13]. Some modern models are designed mainly for rescuing and firefighting purposes, which include the AVIC AG-600 developed by China (the largest amphibious aircraft in-service to date) and the ShinMaywa US-2, a short takeoff and landing (STOL) amphibious aircraft by Japan. Such a vehicle can also provide an alternative mean of cargo and passenger transportation, which is the objective of the recent development of AirFish 8, a WIG aircraft.

Table 1: A chronological list of important amphibious marine vehicles. (AP = Amphibian. FP = Floatplane.)

Year	Model	Country	Vehicle Type
1919	Vickers Viking	Britain	AP
1949	Grumman HU-16 Albatross	USA	AP
1951	DHC-3 Otter	Canada	FP
1965	DHC-6 Twin Otter	Canada	STOL FP
1976	Boeing 929 Jetfoil	USA	Hydrofoil
1984	Dornier Seastar	Germany	Utility AP
2001	AF8-001 (Airfish 8)	Germany	WIG Craft
2003	ShinMaywa US-2	Japan	STOL AP
2007	LISA Akoya	France	Hydrofoil AP
2017	AVIC AG600 Kunlong	China	AP

1.1 Challenges in Amphibious Marine Vehicle Development

Although some of the earliest prototypes were developed mainly during World War I, the systematic study of amphibious marine vehicles was not reported until the World War II era with a focus on hull design [14, 15]. Following the traditional approaches in aircraft design that were common in that era, an amphibious marine vehicle hull was typically designed based on past experiences and by following a trial-and-error procedure, that is, by developing several dynamically similar models

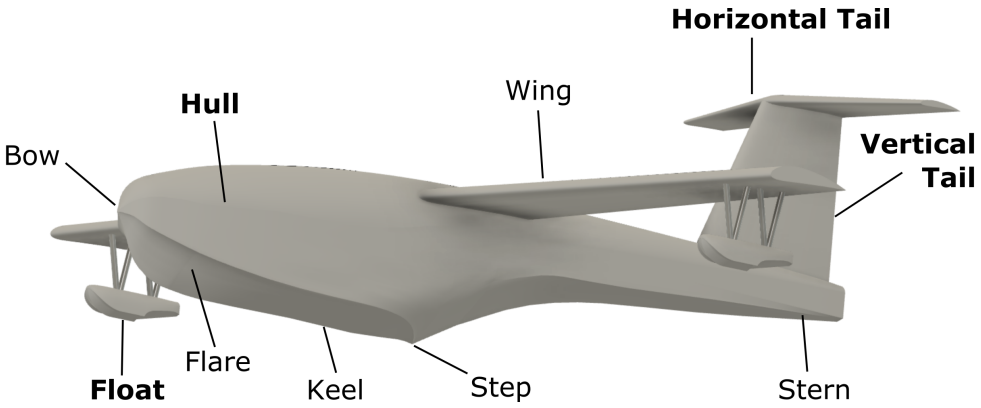

Figure 1: A simplified schematic showing some important components of an amphibious aircraft. Components marked with bold texts indicate a whole component that might contains several sub-parts (e.g., a hull means the whole aircraft fuselage), while those with normal text refer to sub-parts (e.g., a bow is the front part of the hull).

and selecting the best design upon performing towing and flight tests [16]. This process could be extremely costly and time-consuming, in addition to being subjective and lacking theoretical rigor. During the long dormancy since late 1950s until the development of amphibious marine vehicle re-evolves in recent years, the research methods remain largely unchanged [17]. As part of these limitations, the importance of hydrodynamic performance is not well considered apart from the conventional aircraft perspectives [18, 19], which notably slows down the progress of amphibious marine vehicle development.

In amphibious marine vehicles, the hull (i.e., the equivalent of fuselage in conventional aircraft) is the primary contacting part with water during water takeoff and landing. Hence, its shape and form must be properly designed and investigated for more efficient takeoff and landing performances, while maintaining a low aerodynamic drag particularly during cruise. During water takeoff, the peak hydrodynamic resistance of the hull can exceed cruise drag, and the amount of lift generated by the hull can account for 50% to 90% of the hull weight [20]. This hydrodynamic resistance can be the limiting factor of the required thrust-to-weight ratio, which in turn affects the engine selection. A bigger engine is in general heavier, thereby reducing the overall fuel efficiency of the aircraft. In addition, amphibious marine vehicles are often exposed to rough sea and, therefore, they must have a good balance between sea-keeping capabilities and calm-water performance [21]. Furthermore, the hull geometry imposes constraints to the aerodynamic configuration, such as trim limits of stability and center-of-gravity position [22]. With the aforementioned challenges and design considerations, it is imperative to systematically study the hydrodynamic characteristics of amphibious marine vehicle hulls [23], which has a system-level influence on the vehicle design and performance.

However, designing a hull shape consists of time-consuming and cost-expensive operations, primarily due to coupled aerodynamic and hydrodynamic analysis for the takeoff and landing

stages [24]. Hull performance can be assessed either experimentally [25, 26], computationally [27, 28], or by a combination of the two [29]. Numerical simulations are typically unable to resolve a detailed bow wave due to limited grid fineness and will underestimate planing effect because of numerical ventilation [28]. Hence, to date, experimental methods are still the preferred assessment method in this particular context due to its superior reliability and accuracy.

1.2 Past Experimental Practices

With inspiration from the naval architecture research community, the hull experiment is usually conducted in a towing tank, which was first proposed by the National Advisory Committee for Aeronautics (NACA) in the 1950s. The commonly adopted procedures for the test is NACA TN-2503 [30], which was first introduced in 1951. Hereafter, this class of methods will be referred to as "NACA51" for short.

Usually, a scaled-down model of the hull prototype is used for the experiment. A prescribed lift is unloaded to the hull to emulate the lift generated by the actual wing. During the towing procedure, the hull is free-to-trim and heave (or "free-running", with two degrees-of-freedom of translation in z-axis and rotation about y-axis). An example of the application of such method on a particular hull can be found in NACA TN-2481 [22]. To date, most experimental amphibious marine vehicle hull studies still adopt this method [17], albeit with more modern experimental facilities.

Despite its long-standing existence, NACA51 has several shortcomings. The most noticeable one is the lack of proper modeling of the effect of aerodynamic and hydrodynamic coupling. Since the hull is free-running during the towing procedure, parabolic unloading is applied to replace the aerodynamic lift generated by the wing, as lift is proportional to the square of speed ($L \propto V^2$). However, this does not accurately model the lift, due to the mismatch in lift curves between the actual and scaled-down wing. In addition, when the trim angle varies with speed, the lift coefficient also varies with angle-of-attack, which makes the lift dependent on the actual trim angle instead of the initial value. Such a lift unloading setup, which fails to model the actual lift, will lead to an inaccurate free-running resistance curve. This can cause some inaccuracy when evaluating the hump resistance (maximum hydrodynamic resistance), which hinders the correct evaluation of the thrust required during takeoff. Furthermore, it also makes determining the correct hydrodynamic and aerodynamic force attributions from the hull and wing challenging. Last but not least, the hydroplaning force (lift) generated by the hull cannot be measured under this setup, as the heaving motion is not constrained. Hydroplaning force for a high-speed planing hull is not negligible. On the contrary, this force supports up to 90% of the hull weight in some cases [20]. The above-mentioned three problems hinder some generic analyses—such as those of the wave-making resistance, hydroplaning force, spray patterns, etc.—on the hull hydrodynamics, thereby posing considerable challenges in optimizing the hull shape,although hull aerodynamics is also a concern.

1.3 Objective and Structure of the Paper

In summary, the re-emergence of amphibious marine vehicle markets and its contemporary development require an improved, more systematic testing and analysis method for hull hydrodynamics. To address the above-mentioned drawbacks in the NACA51 method, we develop an improved experimental framework that can isolate and accurately measure the hydrodynamic performance of the hull. The details of the improved framework and the results of implementation of the new framework are summarized in this paper.

Specifically, a full experimental framework to determine the hydrodynamic performance of an amphibious marine vehicle hull is introduced in Section 2. An improved decoupled method is used to test the hull hydrodynamic performance without influence from aerodynamic effects. Section 3 explains the detailed procedure of the experiment. The results obtained from the experiment are presented and analyzed in Section 4. Lastly, we present the conclusion in Section 5.

2 Towards a multidisciplinary experimental framework for amphibious marine vehicle design

Given the more complicated operational environments, designing an amphibious vehicle requires the consideration of a hydrodynamic discipline in addition to the disciplines that are common in the design of a conventional aircraft, such as aerodynamics (with the detailed assessments of lift and drag polar), propulsion system, structures, weight and balance, etc. While aerodynamic models with various levels of fidelity have been well-established, hull hydrodynamics (specifically for amphibious marine vehicle) are much less so. Evaluating the hydrodynamic performance of a hull requires quantification of total resistance, hydroplaning lift, buoyancy, and trimming moment. Deriving such an accurate and yet economically feasible hydrodynamic model requires the combination of experimental data (which are accurate but expensive) and numerical simulations (which are more computationally efficient but still lack the required level of fidelity, owing to the limited development as previously mentioned). Using this approach, the model can take advantage of the scalablility of computer simulations with support from the objectivity of experimental data. The envisioned comprehensive design framework is illustrated in Fig. 2. As shown in this figure, experimental results, once validated, will be combined with hydrodynamic simulation results to yield a data-driven hydrodynamic explanatory model. The model will then be used in conjunction with other disciplinary models in the conceptual design stage of an amphibious marine vehicle. The work presented in this paper, however, is focused only on the experimental part of the work. The development of the final scheme is beyond the scope of this work.

2.1 The Improved Experimental Framework

The improved experimental framework provides an efficient testing method that is able to isolate and quantify the hydrodynamic performance of the hull, by a series of towing tank tests. A fixed-trim procedure is adopted, i.e., the hull is fixed onto the towing carriage, to enable obtaining prior information about the hull's attitude, including displacement, draft, trim angle, etc. In addition,

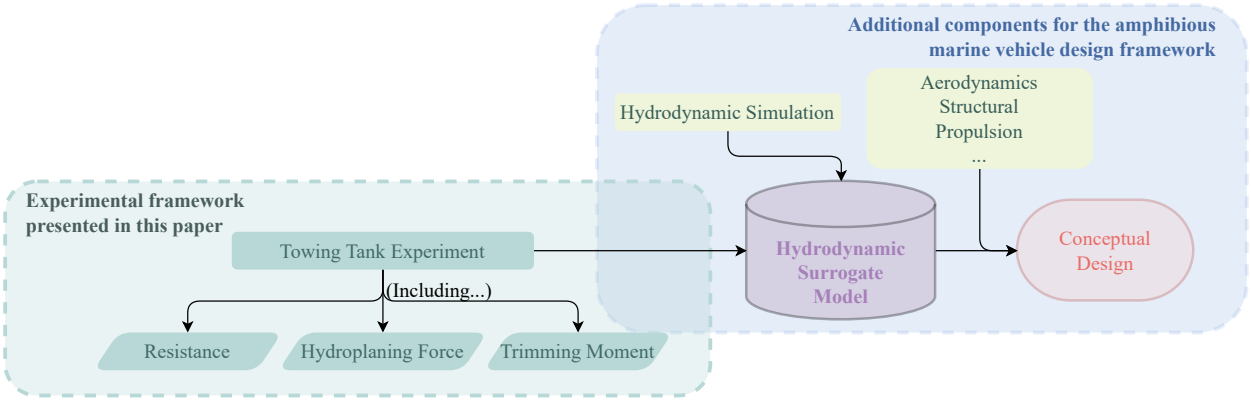

Figure 2: An overview of the proposed amphibious marine vehicle design framework.

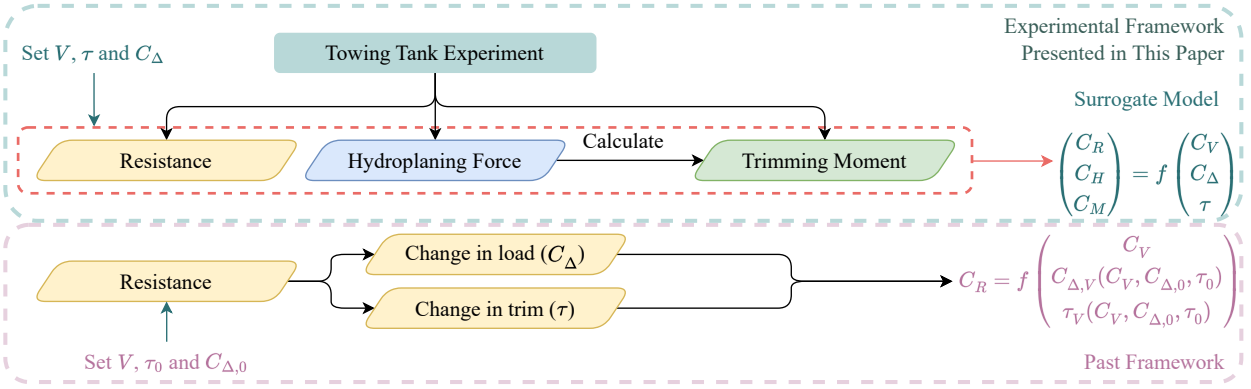

Figure 3: Comparison between the proposed framework and past practices.

hydroplaning force and trimming moment due to an uneven pressure distribution on hull lower surface can be measured and studied. The workflow depicted in Fig. 3 further elaborates the experimental framework and shows a comparison between the proposed framework and traditional practices. Results obtained by this setup can be easily compared with numerical simulation at a reduced computational cost. Due to its fixed setup, a more direct extrapolation law can be used to infer the actual performance of the hull prototype. In this framework, experimentally obtained data do not need to be as dense and extensive as one would need for a dataset capable of directing engineering design. Instead, the experimental results will be used to validate and augment those retrieved by means of computation. In other words, the experimental results guide the setup and refinement of computations and numerical optimizations, instead of directly lead to the design of amphibious marine vehicle itself.

Specifically, the experiment aims to determine how hydrodynamic resistance R, hydroplaning lift H, and trimming moment M vary with speed V, load/buoyancy Δ, and trim angle τ. The experiment is designed to be as comprehensive as possible under budget constraints, in which multiple operating conditions are tested to explore the characteristics of the behavior of the hull.

Mathematically speaking, the experiment attempts to obtain the following mapping

$$\begin{bmatrix} C_R & C_H & C_M \end{bmatrix}^\top = f\left(\begin{bmatrix} C_V & C_\Delta & \tau \end{bmatrix}\right)^\top \tag{1}$$

where forces (R, H, Δ) are non-dimensionalized as $C_{[\cdot]} = \dfrac{[\cdot]}{\rho g b^3}$, moment by $C_M = \dfrac{M}{\rho g b^4}$, and speed by $C_V = \dfrac{V}{\sqrt{gb}}$. In this calculation, ρ, g, and b denote density of water, gravitational acceleration, and the maximum beam (width) of the hull, respectively.

By varying C_V, τ, and C_Δ, scattered values in three dimensions can be obtained to analyze the takeoff dynamics. It is best to distribute experimental conditions to cover all operating scenarios to study the actual situation when motions of the vehicle are not constrained and additional aerodynamic loads are applied.

In the experiment, four waterline heights and five speeds are selected for testing, while maintaining the trim angle at 6°, which is a typical takeoff condition. A more exhaustive design of experiments setup can be performed for more combinations of independent variable values when time and resources allow.

In our proposed framework, the experiment part only focuses on the hull hydrodynamics, but does not aim to resolve the unsteady motion of the hull. In contrast, using the traditional experimental scheme, the transient motion of the hull model (e.g., porpoising, heaving) can be observed directly, though proper conversion is still needed to reflect the behavior of the hull prototype. To evaluate the overall takeoff characteristics of an amphibious aircraft using our framework, the aerodynamic performance of other aircraft components (e.g., wing, tail) should be included, in addition to the hydrodynamic performance of the hull prototype (as introduced in this section). The aerodynamic performance can be obtained by performing wind tunnel testing on the scaled-down model by controlling Reynolds number, or via running a computer simulation of the full-scale prototype, which is a well-established and validated procedure. Having obtained data from both disciplines, the overall aircraft dynamics can be studied by numerically solving the equation-of-motions of the aircraft operations, which is typically formulated as a set of ordinary differential equations. Notwithstanding, this is beyond the scope of current paper;we will leave it for our future studies.

2.2 The Associated Three-Dimensional Extrapolation Method

To be compatible with the improved experimental framework, a modified three-component extrapolation method is derived, which requires three individual resistance components to be scaled separately. The modified method originates from the International Towing Tank Conference in 1978 (ITTC-1978) [31] three-dimensional drag breakdown method, which is still the guideline widely adopted today [32]. The equation of the break down method reads as

$$\begin{aligned} R_m &= R_w + R_f + R_{\text{vp}} \\ C_m &= C_w + C_f + C_{\text{vp}}, \end{aligned} \tag{2}$$

where R_m is the total measured resistance (the subscript $[\cdot]_m$ denotes the scale-down "model"), R_w is the inviscid wake-making resistance of the hull, R_f is the viscous friction drag, and R_{vp} is the viscous pressure drag. Their corresponding non-dimensionalized coefficients ($C_{[\cdot]}$) are obtained by dividing the forces ($R_{[\cdot]}$) by $(1/2)\rho S_{\text{wet}} V^2$, where S_{wet} and V refer to wetted surface area and speed, respectively, and ρ is as previously defined. The friction resistance can be calculated by using the ITTC-57 flat plate friction formula [33], which assumes a simplified hull geometry, as shown below,

$$C_f = \frac{0.075}{(\log \text{Re} - 2)^2}, \tag{3}$$

where $\text{Re} = \frac{\rho V L}{\mu}$ is the Reynolds number. Here, L is the characteristic length, taken to be the length of the waterline, and $\mu = 8.9 \times 10^{-4}\,\text{Pa} \cdot \text{s}$ is the dynamic viscosity of water. Following the ITTC-78 powering performance procedure, the viscous pressure term C_{vp} is often absorbed into the calculation of the friction drag by a form factor $(1 + k)$,

$$C_f + C_{\text{vp}} = (1 + k)C_f. \tag{4}$$

For planing hulls featured by many high-speed marine vehicles, ITTC recommended resistance test procedure in 2002 [34] and suggested that $(1+k) = 1$, which essentially ignores the viscous pressure term. This decision was made based on the findings that the wetted surface area and planing mode are highly dependent on speed, which makes the form factor unreliable to use. Referring to Eq. (2), the ITTC-78 three-dimensional decomposition method for high-speed planing hull is equivalent to ITTC-57 two-component decomposition, which is also known as Froude's decomposition. By combining Eqs. (2) and (4), we can obtain

$$R = \frac{1}{2}\rho V^2 S_{\text{wet}}(C_w + C_f). \tag{5}$$

However, the experiment result shows that for a hydroplaning amphibious aircraft hull, R_m is not proportional to V^2, which means the resulting resistance coefficient is not invariant. In other words, the non-dimensionalized coefficient ($C_{[\cdot]}$) is dependent on the speed. Moreover, S_{wet} also varies with speed but its measurement can be very challenging (will be further discussed in Section 4.2). The fact that all variables in Eq. (5) except ρ are speed-dependent and some are difficult to measure makes accurately estimating resistance very challenging.

We notice that for the same Froude number Fr, by definition $V^2 \propto \lambda$ and $S_{\text{wet}} \propto \lambda^2$, where λ is the scaling factor. We can conclude from Eq. (5) that, for a given Fr number, $R_w \propto \lambda^3$. This scaling method also yields a scaling factor of λ^3, which accords with the two-dimensional extrapolation method [35]. Since $\lambda \sim b$, the wave-making resistance coefficient can be defined as $C_R = \dfrac{R_w}{\rho g b^3}$. Eq. (5) then becomes

$$R = \frac{1}{2}\rho V^2 S_{\text{wet}} C_f + \rho g b^3 C_R. \tag{6}$$

To extrapolate the total resistance for a prototype, both skin friction coefficient of the model

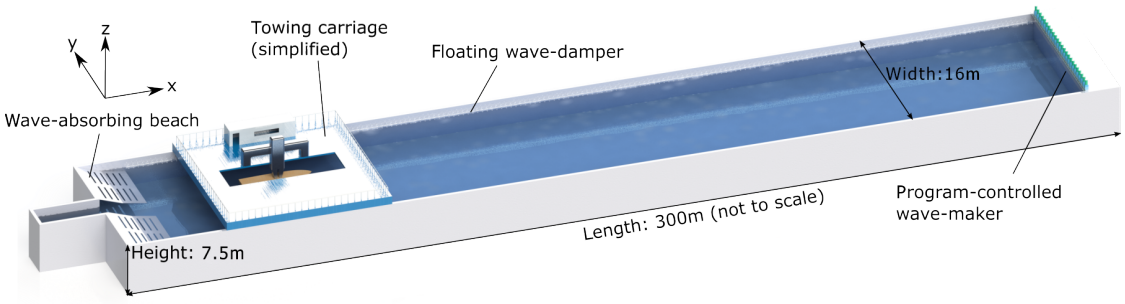

Figure 4: Simplified schematic diagram showing the experimental facility and model assembly.

C_{fm} and wave-making resistance coefficient of the model C_{Rm} needs to be evaluated. Having obtained C_{fm} by utilizing Eq. (3), C_{Rm} can be evaluated by the following equation,

$$C_{Rm} = \frac{R_m - \frac{1}{2}\rho_m V_m^2 S_{\text{wet,m}} C_{fm}}{\rho_m g b_m^3}. \tag{7}$$

Similarly, the same relationship holds true for the wave-making resistance coefficient of the prototype C_{Rs}, which reads as

$$C_{Rs} = \frac{R_s - \frac{1}{2}\rho_s V_s^2 S_{\text{wet,s}} C_{fs}}{\rho_s g b_s^3}. \tag{8}$$

Due to the Froude's similarity, $C_{Rs} = C_{Rm}$ for the same speed and load coefficients. By equating Eq. (7) and Eq. (8), the total resistance of the prototype (denoted by $[\cdot]_s$) can be expressed as

$$C_{Rs} = \frac{\rho_s b_s^3}{\rho_m b_m^3}\left(R_{tm} - \frac{1}{2}\rho_m V_m^2 S_{\text{wet,m}} C_{fm}\right) + \frac{1}{2}\rho_s V_s^2 S_{\text{wet,s}} C_{fs}. \tag{9}$$

Eq. (9) is the final equation to convert experimental data for the model to the predicted data for the prototype.

3 Experiment Implementation

To implement and compare the improved experimental framework and the data extrapolation method against traditional methods, a series of towing tank tests are conducted with a classical and widely used model described in NACA TN-2481 [22] (the NACA TN2481 model hereafter). We choose this particular hull mainly for two reasons. The hull form is a representative single-step planing-tail amphibious aircraft hull that is favorable for modern high-speed applications. In addition, its performance data obtained by using traditional method are well documented, thereby making comparison studies possible.

3.1 Description of Experimental Facility and Instrumentation

The towing tank used for this experiment is the Multiple functionTowing Tank at the Shanghai Jiao Tong University, Shanghai, China. The tank is 300 m in length, 16 m in width and 7.5 m in depth, featuring a high-speed towing carriage with a maximum speed of 10 m/s. The tank is

equipped with program-controlled wave-makers, a wave-absorbing beach, and wave-dampers, to produce or suppress the free surface wave as required by the experimental setup. This facility can and has been widely used to perform an extensive range of oceanic engineering experiments, including performance of underwater vehicles[36], multiple function platforms[37], renewable energy systems[38, 39, 40] and fundamental oceanography [41, 42]. A simplified schematic diagram showing the experimental facility and model assembly is depicted in Fig. 4.

Force data are measured with two Kyowa LSM-B-200NSA1 three-component force transducers, each being rated with 200N maximum capacity and ±0.5% nonlinearity. Their output coefficients and intercepts are calibrated with various check weights. A single MCD-8A eight-channel signal conditioner system is used as the amplifier to the output analog signal from force transducers. Moment is not directly measured but calculated from the force couple, based on the information of the force on each sensor and their distance. A Canon EOS 60D digital single-lens reflex camera is mounted on a tripod, installed on the observation deck of the towing carriage. An additional XIMEA MQ013RG-ON high-speed camera capable of recording 1280p videos at 210 frames per second is also mounted to the observation deck. The distance between the observation deck and the hull model can be electronically adjusted to suit different visualization purposes.

3.2 Hull Model

The 1:1 NACA TN-2481 model is made of glass fiber reinforced plastic (GFRP) in a semi-monocoque structure, to reduce weight while ensuring the necessary rigidity of the structure. The lightweight structure is to facilitate simulating the takeoff scenario near the get-away speed while protecting the sensor. At this speed, the model is tested with low buoyancy, hence the surplus weight has to be supported by the sensors mounted on the top surface of the hull. Following the common practice in naval architecture, it is desired to let the model weight equal to its displacement, so that a full measurement range of the sensor can be utilized. As the model will be fixed to the towing carriage, several waterlines inclining at a prescribed trim angle are marked with laser beams. Table 2 and Figs. 5a and 5b illustrate some of the principal dimensions of the hull. Fig. 5c depicts the fabricated hull used in this experiment and the assembly connecting to the towing carriage.

Table 2: Principal dimensions of the hull model.

Modified TN-2481 Hull	
Length (m)	3.15
Length of forebody (m)	1.32
Length of aftbody (m)	1.83
Beam (m)	0.39
Height (m)	0.54
Weight (kg)	38.0
Draft (m)	$0.065 \sim 0.215$

3.3 Assembly Setup

The hull model is fixed to the towing carriage following the schematic shown in Fig. 4. An upper column is bolted to the towing carriage with no degree-of-freedom (DOF) and two lower columns are bolted to two three-axis force sensors which are fixed to the hull, also with no DOF. In other words, the altitude and motion of the hull are fully constrained and only follow the motion of the towing carriage. The x-velocity of the hull is controlled by the towing speed and the z-position (also waterline height) is adjusted by a system on the towing carriage which can be electrically adjusted in the z-direction. Since the hull is constrained, the two sensors can measure the forces as follows,

$$\begin{aligned} F_x &= F_{x_1} + F_{x_2} = R, \\ F_y &= F_{y1} + F_{y_2} = 0, \\ F_z &= F_{z1} + F_{z2} = H. \end{aligned} \tag{10}$$

The net force in x-direction measures resistance R while the net force in z-direction measures hydroplaning force. The side force in y-direction should diminish due to symmetry.

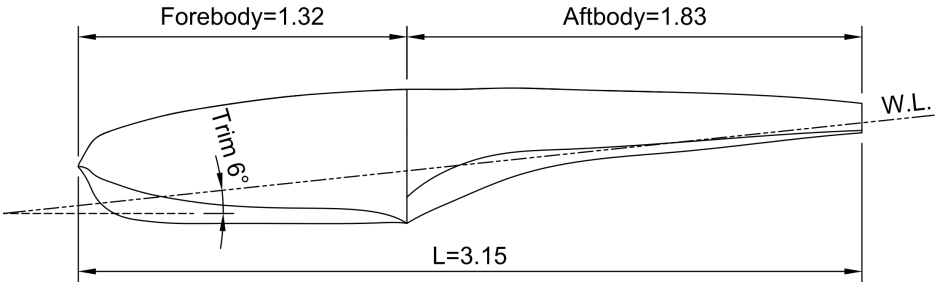

(a) Simplified schematics showing principal dimensions (SI units) of the hull model. Side view.

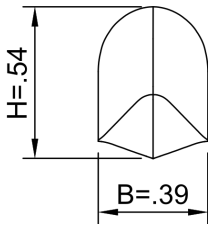

(b) Front view.

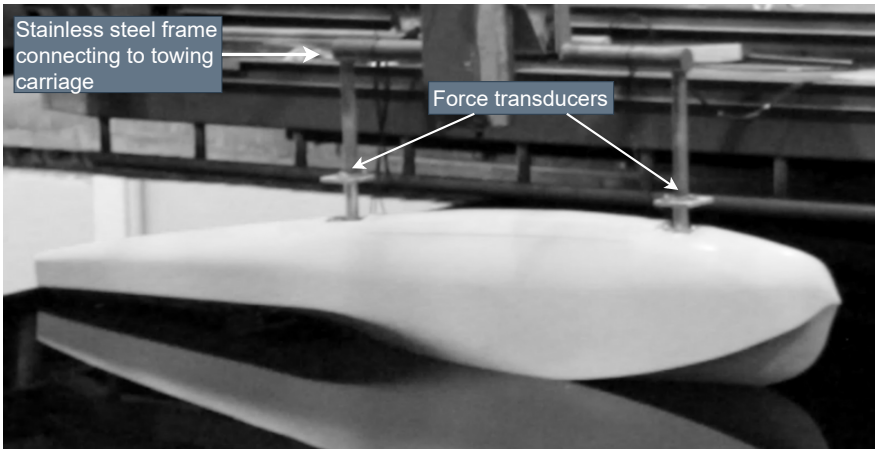

(c) The fabricated hull model and assembly used for the experiment.

Figure 5: Description of the modified TN-2481 hull model.

3.4 Experimental Scenarios

The experimental setup is focused on studying the hydrodynamic effect, while considering the aero-hydrodynamic coupling within the system. To demonstrate the advantage of the improved framework and systematically evaluate the hull performance, we plan the testing scenarios based on realistic operational conditions. The design and operating parameters are determined to reflect the operations of an amphibious aircraft to which the hull will be fitted, following a previous work by one of the authors [24].

With the above considerations, trim angle τ is set to be 6°, corresponding to the takeoff altitude of the aircraft model, limited by the sternpost angle. The maximum load coefficient C_Δ being tested is 1.35, representing the maximum takeoff weight, while the minimum is set to 0.27, below which value the model is hardly contacting water. The speed coefficient is tested up to $C_V = 2.56$, at which speed most of the weight is already carried by the aerodynamic lift. Hence, conditions at both high speed and large displacement are not tested, because these conditions are unlikely to occur in real-life operations. These values are determined based on the aerodynamic analysis of an amphibious aircraft during the preliminary design phase. Readers are referred to the reference [24] for the details of the procedure, which is beyond the scope of this work.

4 Results and Discussions

In this section, we analyse the hydrodynamic performance of the TN2481 hull, focusing particularly on resistance, hydroplaning force, and bow wave, which are obtained by using the developed experimental framework. First, we demonstrate the challenges that the traditional non-dimensionalization technique imposes on the data extrapolation of an amphibious hull. We then use the proposed non-dimensionalization method to conduct further analyses on the resistance and hydroplaning force coefficients. The captured flow field and bow wave are then used to explain the force characteristics. It is worth noting that during the actual experiment, testing speed range is smaller for large displacement values ($C_\Delta = 0.95$ and $C_\Delta = 1.35$), due to the reason mentioned in Section 3.4.

4.1 Traditional Resistance Coefficient

Traditionally, as a common practice in fluid dynamics, resistance is non-dimensionalized as $C_D = \frac{2R}{\rho V^2 S_{\text{wet}}}$[1]. However, as mentioned in Section 2.2, such a calculation is particularly difficult for a hydroplaning amphibious hull, mainly for two reasons. First, there is no agreement on the scale length for the amphibious marine vehicle when we calculate Fr number. On the one hand, the distance between perpendiculars (L_{pp}) varies with the displacement for this type of hull (as opposed to the hull of a container ship) and hence, scaling the velocity by $\text{Fr} = \frac{V}{\sqrt{gL_{\text{pp}}}}$ is not consistent. On the other hand, if hull length L is used instead of L_{pp} to ensure a constant characteristic length, the physical meaning of Fr number disappears. Using speed coefficient $C_V = \frac{V}{\sqrt{gb}}$ suggested in [22]

[1] To better distinguish the mathematical definition of the traditional resistance coefficient and the proposed one, we denote the traditional one by C_D and proposed one by C_R, respectively.

eliminates this problem. Secondly, S_{wet} changes with velocity, thereby making its measurement difficult and unreliable [34].

To demonstrate the above statement, assuming S_{wet} can be determined by the initial displacement, we plot C_D against C_V in Fig. 6. It shows that C_D notably increases with C_V at lower speed, then gradually drops asymptotically to some extent. At a lower speed, this is consistent with the typical resistance characteristic of a planing hull, which reaches its hump speed at $C_V = 1.13$. However, beyond hump speed, a notable decrease in resistance coefficient is contrast to a typical planing hull [28, 43, 44], which might be due to a reduced S_{wet} in reality.

One can find that if we were to scale hydrodynamic forces from the model to the prototype in the traditional way, where Fr and S_{wet} are difficult to determine and C_D non-constant, uncertainty and error larger than expected may occur in the extrapolated value. In this paper, we propose to use the force coefficient $C_{[\cdot]} = \dfrac{[\cdot]}{\rho g b^3}$ and speed coefficient C_V instead. By doing so, we can obtain the proposed $C_R = \dfrac{R}{\rho g b^3}$.

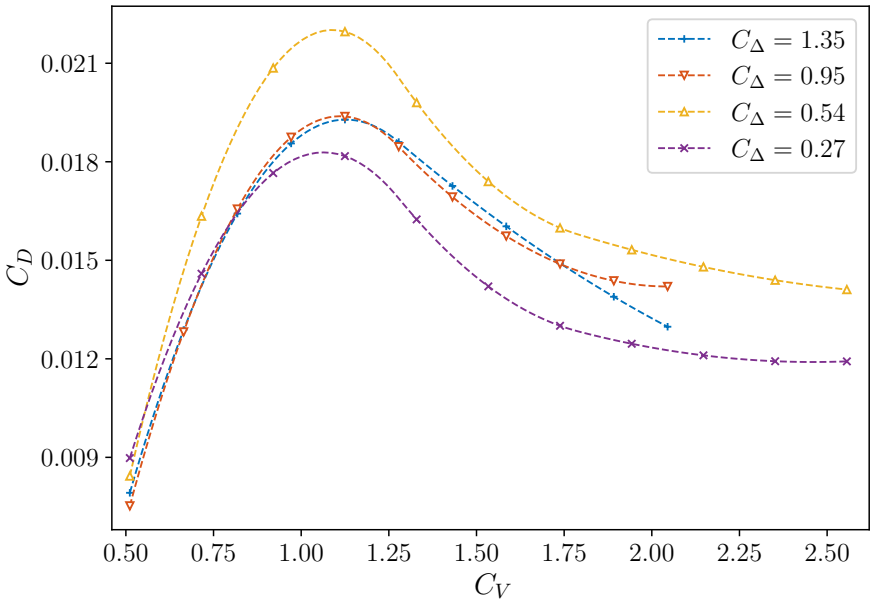

Figure 6: C_D against C_V under various C_Δ, $\tau = 6°$.

4.2 Modified Resistance Coefficient

Having explained drawbacks with C_D, we now shift our attention to C_R. We study the variation of C_R as a function of C_V under various drafts, using the proposed framework, when the trim angle $\tau = 6°$. This variation is visually presented in Fig. 7. It can be observed that under a given draft, resistance is not proportional to the square of speed. Instead, Fig. 7 shows that C_R exhibits a linear relationship with respect to C_V. The relationship between C_R and C_Δ is shown in Fig. 8, where a quadratic trend is displayed. Such relationships suggest that the empirical scaling equation $C_{R\Delta} = C_R \cdot (C_\Delta / C_{\Delta_0})$ used by Gudmundsson [45] is insufficient and, therefore, requires

some modification. We believe that the observed linear relationship may be due to a reduced S_{wet} and can be explained by the bow wave pattern, which will be discussed shortly.

Resistance and trim curves documented in NACA TN-2481 using NACA51 framework are overlaid on Fig. 7 (denoted as $C_{\Delta,0}$ in the legend, shown in olive green and brown) for comparison purposes. Note that, due to the free-running setup in NACA51, τ and C_Δ of the hull could not be controlled. The measured τ is plotted in brown. What causes this notable difference is that, the resistance data obtained under the proposed framework reflect only the hydrodynamic performance of the hull model, while the NACA51 data are influenced by both the natural hydrodynamic force and an artificial aerodynamic loads.

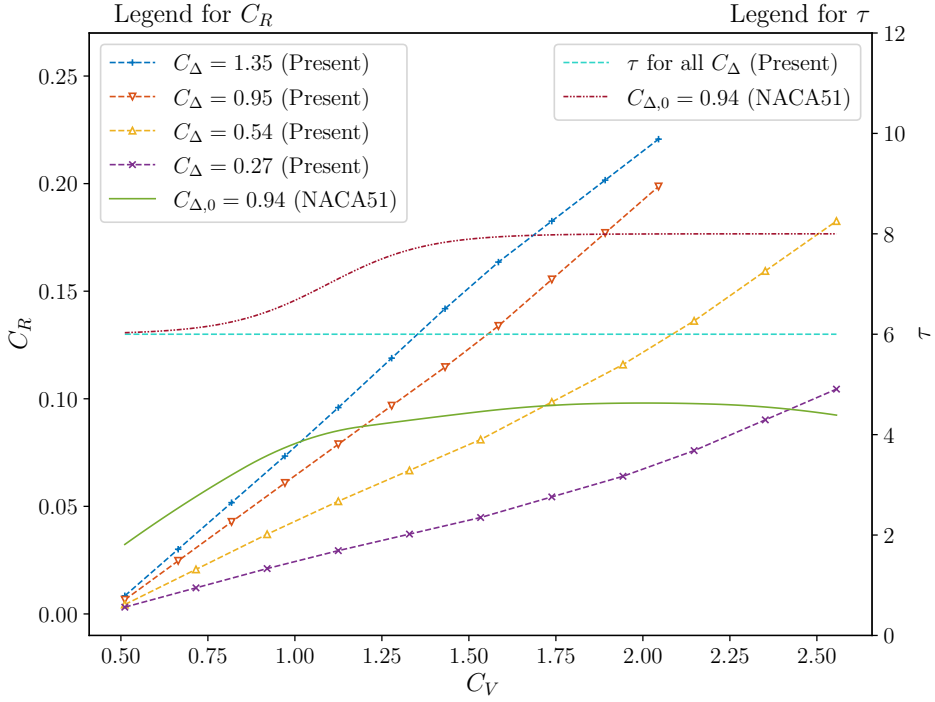

Figure 7: C_R against C_V under various C_Δ, $\tau = 6°$. Resistance and trim curve documented in NACA TN-2481 using NACA51 framework is plotted for comparison.

With both C_Δ and τ controlled, the Cartesian experimental dataset used in our framework can be conveniently used to derive a data-enhanced model for the hull hydrodynamic performance. For example, a regression model can be useful during the preliminary design and sizing of the amphibious marine vehicle. The following regression formula can model such a relationship with reasonable accuracy, as assessed by a coefficient of determination of $R^2 = 0.995$,

$$C_R = (BC_V + C)(DC_\Delta^2 + EC_\Delta + F), \tag{11}$$

where empirical coefficients B, C, D, E, and F are determined by the Levenberg-Marquardt algorithm. The regression equation is formulated based on our previous observation on the relationships between C_R, C_V, and C_Δ; Eq. (11) is shown to have the best performance among other formulas

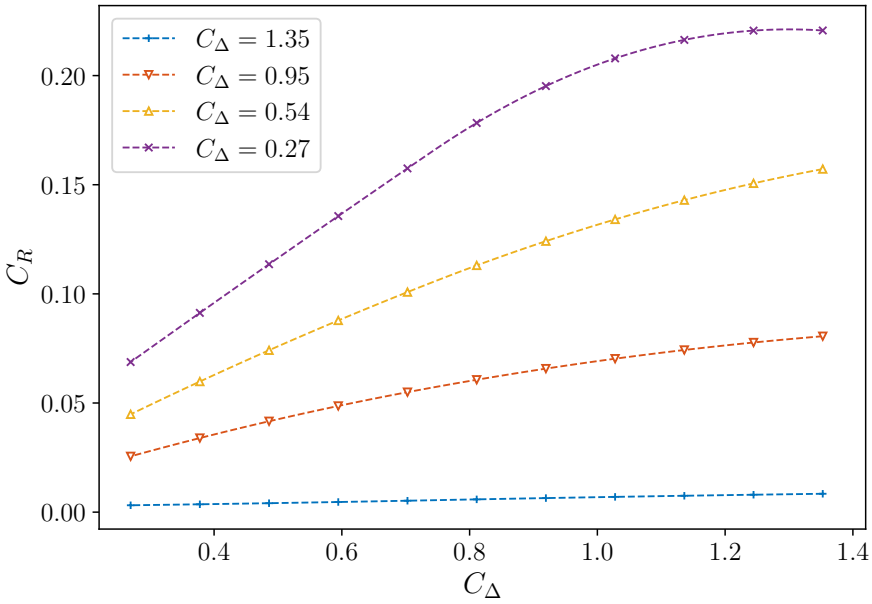

Figure 8: C_R against C_Δ at various C_V, $\tau = 6°$.

attempted. In this study, they are given as

$$B = -0.0876, \quad C = \quad 0.0411,$$
$$D = \quad 0.6674, \quad E = -2.0944, \quad F = -0.0167.$$

With Eq. (11), one can study the relationship among C_V, C_R, and C_Δ in greater details as shown in Fig. 9. For example, it is possible to use this regression model to predict the critical speed for the hull to enter planing mode, given an initial takeoff weight.

Another important but often-missed contributing factor to the hydrodynamic resistance is the bow wave (Fig. 10). One can see that the incoming flow is repelled sideways from the hull due to the hull flare and spray rail, forming a strong bow wave. Table 3 tabulates the relation between the bow wave height (marked with H in pink Fig. 10) and the speed. We also discover that the submerged volume of the hull is reduced near the step due to the wake. As the cross-sectional area of the hull does not increase towards the aft-body like a traditional boat hull does (rather, the hull becomes much narrower after the step), water repelled away from the hull reduces S_{wet}. When speed increases, S_{wet} decreases, thus frictional resistance decreases, but bow wave grows stronger and wave-making resistance increases, causing the overall resistance not proportional to V^2. In this experiment, S_{wet} is qualitatively determined by visual observations from outside of the model, a common procedure by ITTC [34], as the quantity of interest C_R does not depend on S_{wet}. In the case where running S_{wet} (at high speed) must be quantitatively measured when spray occurs, insoluble paint can be applied to the hull body, and S_{wet} is the area where paint dissolves.

It is worth mentioning that C_R in this section refers to the total resistance coefficient (often denoted by C_t) and includes the skin-friction and residual (wave-making) resistance. While the resid-

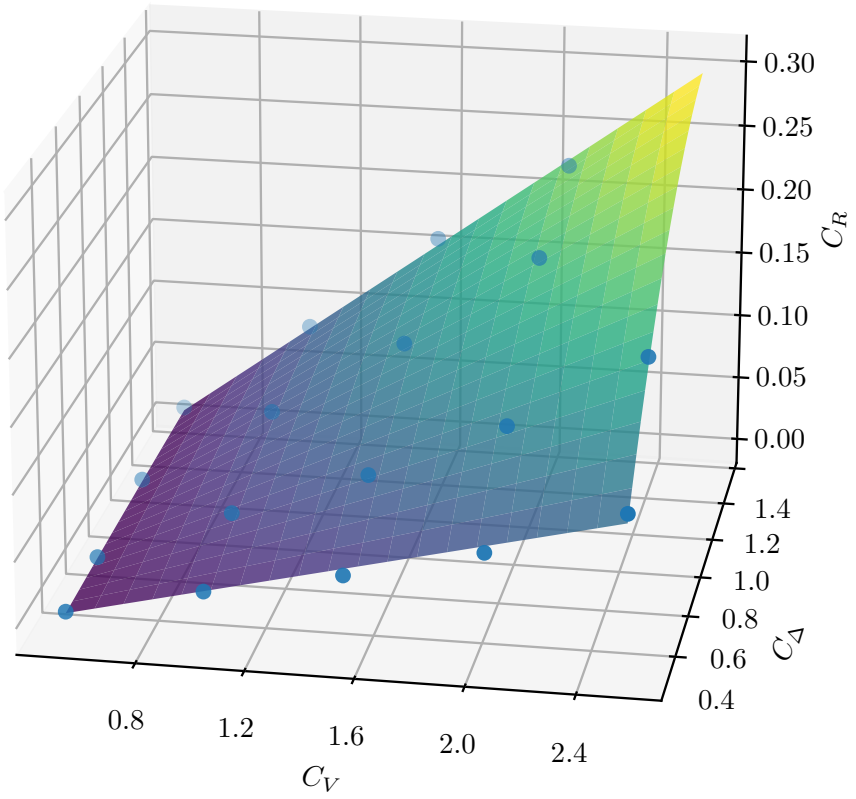

Figure 9: Quadratic fitting of 2-D resistance data with $R^2 = 0.995$.

ual resistance shall also be non-dimensionalized following the proposed approach, i.e., $C_w = \frac{R_w}{\rho g b^3}$, the skin-friction resistance is still evaluated by the ITTC-57 formula (Eq. (3)). The decomposition procedure has been discussed in Section 2.2. The data extrapolation for the preliminary design of an amphibious vehicle system is beyond the scope of the current paper.

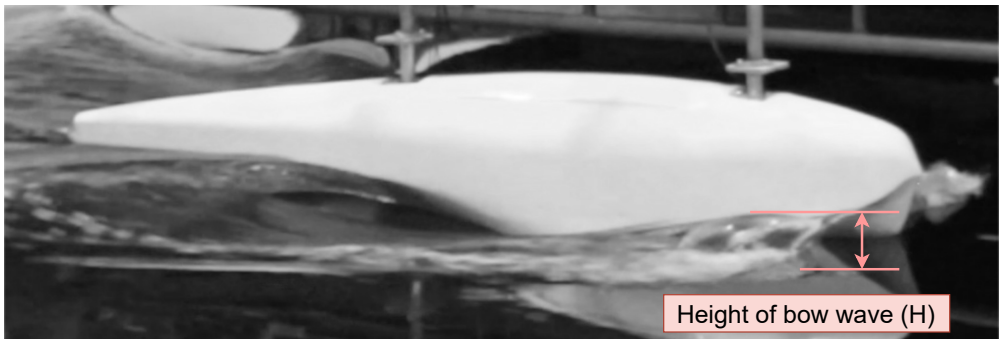

Figure 10: Flow around the hull at draft = -16cm and speed = 2m/s with the bow wave highlighted.

4.3 Lift

Using the improved framework, the hydroplaning force generated by the hull, i.e., lift, can also be measured. Measuring the lift is an essential and yet non-trivial process to validate the design of an

amphibious planing hull that is commonly used in large high-speed amphibious marine vehicles.

Fig. 11 shows the lift curves under various drafts. It can be observed that under a given draft, lift decreases first and then increases. At a lower speed, the hull flare pushes the incoming flow away from the hull body—the same phenomenon previously explained in Section 4.2—causing the submerged volume near the step to decrease. Hence, within this speed range, the measured lift appears to be negative while the hydroplaning effect is still negligible. At a higher speed, hydroplaning force becomes more prominent as it is proportional to the square of speed, which compensates the decreased buoyancy. As a result, a trend of increasing lift appears. When $C_\Delta = 0.27$ and $C_\Delta = 0.54$, although speed is only tested up to $C_V = 2.04$ (due to the reason mentioned in Section 3.4) while C_H is still negative, we can reasonably extrapolate the trend to reach the same conclusion (as when $C_\Delta = 0.95$ and $C_\Delta = 1.35$).

Since the NACA51 framework requires to offload a prescribed aerodynamic load to the hull body and the model is free to heave, it is not possible to isolate and measure hydroplaning lift. As such, a comparison against previous hydroplaning lift data, which were typically obtained based on the NACA51 framework, is not presented here.

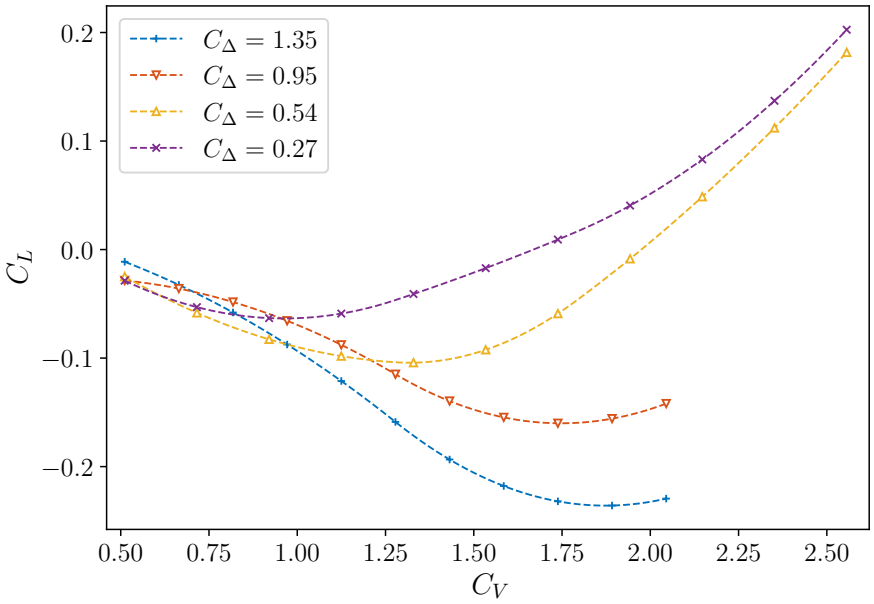

Figure 11: Hydroplaning force (lift) curves under various C_Δ, $\tau = 6°$.

4.4 Spray and Wetted Surface Area

As discussed before, the bow wave, spray, and wetted surface area notably influence the force characteristics. Here, we use these features in the flow field to understand the macroscopic force behaviors.

A significant amount of spray can be observed at the forebody, mainly due to three reasons. First, the warped hull has a V-shaped forebody, leading to a strong effect to push incoming water flow horizontally. At a lower speed, this type of hull usually suffers from a larger resistance compared

to conventional displacement hull. However, as speed increases, the hull is supported by planing force (lift), thereby greatly reducing displacement and, therefore, resistance. Second, forebody spray, especially at a higher speed, appears like a thin sheet of water, because the effect of surface tension is more significant compared to flow momentum. The surface tension also causes spray separation from the hull to be delayed, causing a more apparent visual effect of the spray. At a larger scale, spray is more likely to be in droplets, thereby decreasing the wetted surface area (relative to the whole surface area) compared to model scale. Lastly, to obtain as comprehensive data as possible, the tested speed range is purposely made to exceed the speed profile that an amphibious marine vehicle may encounter during a typical takeoff run, yielding a seemingly oversized spray profile.

From Table 3, we observe that bow wave height and resistance are approximately linear with respect to the speed. Similarly, when $C_\Delta = 0.95$, 0.54, and 0.27, bow wave height is also nearly linear to the displacement. However, when $C_\Delta = 1.35$, the bow wave height is limited by the spray rail, so the measured value is comparable to that at $C_\Delta = 0.95$.

Table 3: Height of bow wave against C_V and C_Δ.

C_V	0.5	1.0	1.5	2.0	2.6
$C_\Delta = 1.35$	2.4	9.8	17.3	22.8	N/A
$C_\Delta = 0.95$	1.4	10.5	16.9	21.3	N/A
$C_\Delta = 0.54$	Negligible	6.3	9.6	17.6	20.0
$C_\Delta = 0.27$	Negligible	5.2	7.6	12.2	14.6

5 Conclusion

In this study, we developed an improved experimental framework and the corresponding data processing method to provide more detailed hydrodynamic performance of amphibious marine vehicles that can address the limitations of existing methods. The framework focuses on the generic hydrodynamic performance of the hull, without aerodynamic interference. The capability of the framework was demonstrated by performing a series of experiments on a classical NACA TN-2481 hull in a towing tank facility. We observed that the resistance coefficient had an almost linear relationship with respect to speed coefficient and was quadratically correlated to displacement; both observations are contrast to the traditional empirical formula. To represent such relationships, we derived an appropriate regression model, using C_R samples obtained from the improved framework, where C_Δ and τ can now be fixed. Deriving such a dynamic model was not possible with the classical NACA51 framework where often only the nominal loading condition was used for testing. To decompose resistance components and to apply the data obtained from a hull model to a full-scale prototype, we developed an improved data reduction (to resolve measured resistance into dimensionless resistance coefficient components) and extrapolation (to convert resistance from model to full scale) method associated with the framework, based on our findings of the resistance coefficient

data. Such data reduction method is also purely for scaling the hydrodynamic performance and is based on Froude's similarity.

Our results also showed that the developed method could accurately evaluate hydroplaning lift, which is a critical feature of an amphibious hydroplaning hull. As such, we successfully addressed another limitation of the NACA51 framework, which could not measure this particular lift component. In particular, the results showcased a dynamic variation of hydroplaning lift and loss of buoyancy against speed, with the planing mode transition occurs at around 60 % of the maximum tested speed (beyond which speed the aircraft weight is mostly carried by the aerodynamic lift).

As stated in Section 3.4, tests with various trim angles can be conducted to determine an optimal takeoff angle-of-attack. In addition, trimming moment due to hydrodynamic loads can be obtained to analyze its dynamic stability. Despite the fact that this framework and the present results are still insufficient to obtain an optimal design of the hull geometry, they will be instrumental in the derivations and validations of suitable numerical models, which will in turn enable performing numerical optimizations. Once established, the dynamic model, in conjunction with other disciplinary models, can be used to build a multidisciplinary design framework to advance the design and development of amphibious marine vehicle design.

Acknowledgments

This work was supported in part by the Hong Kong University of Science and Technology (HKUST) Undergraduate Research Opportunities Program Collaboration Fund under Grant UROPCFS1905 and in part by the HKUST–Shanghai Jiao Tong University Collaboration Fund under Grant WH610160507/035 (SJTU) and Grant SJTU21EG08 (HKUST). The authors would like to thank Mr. Arjit Seth for his valuable discussion when formulating the problem; Hao Xu, Zhipeng Jiang, and Fangyi Wei for participation in the design of the scaled-model and the experiments; and Yinzhong Hu, Dehui Si, Wenping Chen, and their colleagues for the fabrication of the hull.

References

[1] P. Liam, S. Sajad, S. Mae, L. Howard, AUV navigation and localization: A review, IEEE Journal of Oceanic Engineering 39 (2014) 131–149.

[2] Z. Shen, X. Chen, L. Huang, Challenges for aircraft design due to special mission models of large-scale amphibious aircraft, Acta Aeronauticaet Astronautica Sinica 40 (1) (2019) 522400.

[3] A. Fevralskikh, A development of longitudinal static stability analysis method of a wing-in-ground effect vehicle in cruise during the design process, Ocean Engineering 243 (2022) 110187.

[4] Z. Zeng, K. Sammut, L. Lian, A. Lammas, F. He, Y. Tang, Rendezvous path planning for multiple autonomous marine vehicles, IEEE Journal of Oceanic Engineering 43 (2018) 640–664.

[5] J. Manley, Multiple AUV missions in the national oceanic and atmospheric administration, in: 2004 IEEE/OES Autonomous Underwater Vehicles, 2004, pp. 20–25.

[6] M. Maclver, E. Fontaine, J. Burdick, Designing future underwater vehicles: principles and mechanisms of the weakly electric fish, IEEE Journal of Oceanic Engineering 29 (2004) 651–659.

[7] Y. Li, A. Lansburgh, S. Calisal, An integrated approach to increase marine transportation safety in harbor areas, Marine Technology Society Journal 51 (2017) 72–85.

[8] Y. Li, S. Calisal, Numerical simulation of ship maneuverability in wind and current, with escort tugs, Marine Technology and SNAME News 42 (2005) 159–176.

[9] X. Yang, T. Wang, J. Liang, G. Yao, M. Liu, Survey on the novel hybrid aquatic-aerial amphibious aircraft: Aquatic unmanned aerial vehicle (AquaUAV), Progress in Aerospace Sciences 74 (2015) 131–151.

[10] S. Wang, Y. Duan, F.and Li, Y. Xia, Z. Li, An improved radial basis function for marine vehicle hull form representation and optimization, Ocean Engineering 42 (2022) 112000.

[11] W. J. Boyne, American flying boats and amphibious aircraft: An illustrated history, Aviation History 21 (2) (2010) 63–.

[12] R. C. Knott, The American Flying Boat: An illustrated history, Naval Inst. Pr, 1988.

[13] R. Liem, Review of design aspects and challenges of efficient and quiet amphibious aircraft, Journal of Physics: Conference Series 1005 (2018) 012027.

[14] F. W. S. Locke, General resistance tests on flying-boat hull models, Tech. rep., National Advisory Committee for Aeronautics (1944).

[15] F. W. S. Locke, J. A. Barklie, Tank tests on the resistance and porpoising characteristics of three flying-boat hull models equipped with planing flaps, Tech. rep., National Advisory Committee for Aeronautics (1944).

[16] E. G. Stout, Development of high-speed water-based aircraft, Journal of the Aeronautical Sciences 17 (8) (1950) 457–480.

[17] L. Wang, H. Yin, K. Yang, H. Liu, J. Zhu, Water takeoff performance calculation method for amphibious aircraft based on digital virtual flight, Chinese Journal of Aeronautics 33 (2020) 3082–3091.

[18] L. Qiu, W. Song, Efficient decoupled hydrodynamic and aerodynamic analysis of amphibious aircraft water takeoff process, Journal of Aircraft 50 (2013) 1369–1379.

[19] J. Cary, G. Crouse, Preliminary design optimization of an amphibious aircraft, in: 50th AIAA Aerospace Sciences Meeting including the New Horizons Forum and Aerospace Exposition, 2012.

[20] L. J. Doctors, Hydrodynamics of high-speed small craft, Tech. rep., Department of Naval Architecture and Marine Engineering, University of Michigan (1985).

[21] D. Savitsky, P. W. Brown, Procedures for hydrodynamic evaluation of planing hulls in smooth and rough water, Marine Technology and SNAME News 13 (04) (1976) 381–400.

[22] H. B. Suydam, Hydrodynamic characteristics of a low-drag, planing-tail flying boat hull, Tech. rep., National Advisory Committee for Aeronautics (1952).

[23] I. Dathe, M. DELEO, Hydrodynamic characteristics of seaplanes as affected by hull shape parameters, in: Advanced Marine Vehicles Conference, 1989, p. 1540.

[24] A. Seth, R. P. Liem, Amphibious aircraft developments: Computational studies of hydrofoil design for improvements in water-takeoffs, Aerospace 8 (2021) 1–31.

[25] E. G. Stout, Experimental determination of hydrodynamic stability, Journal of the Aeronautical Sciences 8 (2) (1940) 55–61.

[26] R. Van Dyck, Seaplanes and the towing tank, in: Advanced Marine Vehicles Conference, 1989, p. 1533.

[27] P. Lotfi, M. Ashrafizaadeh, R. Kowsari Esfahan, Numerical investigation of a stepped planing hull in calm water, Ocean Engineering 94 (2015) 103–110.

[28] P. Casalone, O. Dell'Edera, B. Fenu, G. Giorgi, S. A. Sirigu, G. Mattiazzo, Unsteady RANS CFD simulations of sailboat's hull and comparison with full-scale test, Journal of Marine Science and Engineering 8 (2020) 394.

[29] C. Judge, M. Mousaviraad, F. Stern, E. Lee, A. Fullerton, J. Geiser, C. Schleicher, C. Merrill, C. Weil, J. Morin, M. Jiang, C. Ikeda, Experiments and CFD of a high-speed deep-V planing hull—Part I: Calm water, Applied Ocean Research 96 (2020) 102060.

[30] W. C. Hugli, W. C. Axt, Hydrodynamic investigation of a series of hull models suitable for small flying boats and amphibians, Tech. rep., National Advisory Committee for Aeronautics (1951).

[31] Propulsion Committee of the 28th ITTC, ITTC – Recommended precedures and guidelines, 1978 performance prediction method, resistance test, Tech. rep., International Towing Tank Conference (2017).

[32] Propulsion Committee of the 29th ITTC, ITTC – Recommended precedures and guidelines, resistance test, Tech. rep., International Towing Tank Conference (2021).

[33] A. Morrall, 1957 ITTC model-ship correlation line values of frictional resistance coefficient, Tech. rep., International Towing Tank Conference (1957).

[34] Propulsion Committee of the 23rd ITTC, ITTC – Recommended precedures and guidelines, testing and extrapolation methods, high speed marine vehicles, resistance test, Tech. rep., International Towing Tank Conference (2017).

[35] J. Carlton, Marine Propellers and Propulsion, Elsevier, 2019.

[36] Y. Xia, K. Xu, Y. Li., G. Xu, X. Xiang, Improved line-of-sight trajectory tracking control of underactuated auv subjects to ocean currents and input saturation, Ocean Engineering 174 (2010) 14–30.

[37] W. Liu, Y. Guo, X.and Li, H. Zhang, G.and Wu, X. Song, Z. Liu, Experimental and numerical investigation on structural response of a fmrc hexagon platform in wave, Ocean Engineering 223 (2021) 108998.

[38] Z. Li, K. Ghia, Y. Li., Z. Fan, L. Shen, Unsteady reynolds-averaged navier-stokes investigation of free surface wave impact on tidal turbine wake, Proceedings of Royal Society, A 229 (2021) 113689.

[39] X. Zheng, G. Chen, W. Cao, H. Xu, R. Zhao, Q. Xu, M. Kramer, D. Le Touzé, A. G. Borthwick, Y. Li, On the energy conversion characteristics of a top-mounted pitching absorber by using smoothed particle hydrodynamics, Energy Conversion and Management 250 (2021) 114893.

[40] Z. Gao, X. Feng, Zhang.Z., Z. Liu, X. Gao, L. Zhang, S. Li, Y. Li, A brief discussion on offshore wind turbine hydrodynamics problem, Journal of Hydrodynamics 34 (2022) 15–30.

[41] T. Tang, D. Xu, W.and Barratt, H. a. L. Bingham, P. Talor, T. van den Bremer, T. Adcock, Spatial evolution of the kurtosis of steep unidirectional random waves, Journal of Fluid Mechanics 908 (2021) A3.

[42] Y. Liu, D. Eeltink, T. Tang, D. Barratt, Y. Li, T. Adcock, T. van den Bremer, Comparison of breaking models in envelope-based surface gravity wave evolution equations, Physical Review Fluids 8 (2023) 054803.

[43] M. B.Tofa, A. Maimun, Y. M.Ahmed, S. Jamei, Take off resistance estimation of wing in ground effect (WIG) craft, in: Proceedings of the 6th Asia Pacific Workshop on Marine Hydrodynamics (APHydro), 2012, pp. 1–6.

[44] B. Tagliafierro, S. Mancini, P. Ropero-Giralda, J. M. Domínguez, A. J. C. Crespo, G. Viccione, Performance assessment of a planing hull using the smoothed particle hydrodynamics method, Journal of Marine Science and Engineering 9 (3) (2021).

[45] S. Gudmundsson, General Aviation Aircraft Design: Applied Methods and Procedures, Vol. App.C3, Elsevier, 2014.